

# Source of unusual monochromatic wave packets recorded globally in the seismograms of 11 November 2018

S. N. Bhattacharya<sup>1</sup>, V. K. Gahalaut<sup>1,2,\*</sup>, Narendra Pandey<sup>1</sup>, Shankar Pal<sup>1</sup>, Rajeev Manhas<sup>1</sup> and G. Suresh<sup>1</sup>

<sup>1</sup>National Center for Seismology, New Delhi 110 003, India

<sup>2</sup>Present address: CSIR-National Geophysical Research Institute, Hyderabad 500 007, India

**On 11 November 2018, all global seismic stations recorded unusual long-period wave packets without any discernible body waves. Our analyses show that the wave packets are monochromatic with period 15.6 sec and are fundamental-mode non-dispersive Rayleigh waves. Using the arrival times of wave packets, the source is approximately located at the northeastern edge of the recent earthquake swarm zone, off the east coast of Mayotte, a volcanic island between North Madagascar and East Africa. Synthetic seismograms for an isotropic source at 15 km depth with a transient oscillation of the same period as that observed in the wave packets, are consistent with the recorded seismograms. We estimate an equivalent magnitude ( $M_w$ ) of  $\sim 4.8$  for this source and suggest that a volcanic fluid sphere of radius  $\sim 5$  km might have generated such radial oscillations. Interestingly, similar monochromatic waves with lesser amplitude were also recorded on many occasions from the same source during 21 June 2018 to 10 September 2019. The period of waves increased from 15.2 sec in June to 15.6 sec in October–November 2018 and then decreased to 15.0 sec in September 2019, which implies an increase and then decrease in radius of the fluid sphere at the source.**

**Keywords:** Monochromatic wave packets, seismograms, seismic stations, source characterization.

ON 11 November 2018, between 09:30 and 11:30 UTC, all global seismic stations recorded a few minutes long low-frequency wave packets. However, body waves were not visible on the seismograms and as such source parameters, including the location of the event, could not be determined perhaps due to small magnitude or non-double couple source mechanism or some other slow process (e.g. slow earthquakes, landslides, rockfalls, calving events, etc.). The wave packets arriving early at FOMA (in South Madagascar) and KMBO (in Kenya) indicate an approximate source location at Comoros archipelago in the northern Mozambique Channel between

north Madagascar and Mozambique (Figure 1a). The archipelago consists of four principal volcanic islands over a distance of about 300 km, approximately along the WNW-ENE direction<sup>1</sup>. The origin of this archipelago is either a deep mantle plume that developed a hot-spot track from the Seychelles Plateau, or a lithospheric deformation that reactivated transform faults and controlled the magma path<sup>2</sup>. From west to east these volcanic islands are (i) Grand Comore, (ii) Anjouan, (iii) Moheli and, (iv) Mayotte. At Mayotte, the magmatic activity started at least  $\sim 10.6$  Ma ago, and at Anjouan and Moheli  $\sim 5$  and 3.9 Ma ago respectively, and at Grand Comore since  $\sim 0.13$  Ma (ref. 2). Among the four islands, the Grand Comore is the largest, where Karthala is an active shield volcano covering two-thirds of the island area that has erupted more than 20 times since the 19th century<sup>3</sup>. The submarine volcanic island Geiser bank is situated about 150 km northeast of Mayotte (Figure 1a). The Mozambique Channel played a crucial role during Gondwana break-up. It is commonly accepted that break-up between its eastern (Antarctica, Australia, India, Madagascar) and western (Africa, South America) was caused at first by the opening of Mozambique and Somali basins.

Since 10 May 2018, earthquake swarm activity has been reported from off the east coast of Mayotte, where earthquakes are generally rare, as evident from the United State Geological Survey (USGS) earthquake catalogue. The epicentres of the swarm are located in the offshore region extending for about 60 km from the east coast of Mayotte (Figure 1b). This shallow-depth swarm was active during May–June 2018, with the largest earthquake of  $M_w$  5.9 on 15 May 2018 (Figure 1b) with its hypocentre at 12.77°S, 45.58°E and 17 km depth (USGS). Since July 2018, swarm activity has decreased both in terms of frequency of earthquakes and their magnitudes. Considering the current earthquake swarm activity on the east coast of Mayotte, it is logical to assume that the source of the unusual wave packets is likely to be located in the swarm zone. Thus, in this analysis we assumed its source to be located at the epicentre of the largest earthquake of 15 May 2018 with a depth of 15 km.

\*For correspondence. (e-mail: vkgahalaut@yahoo.com)

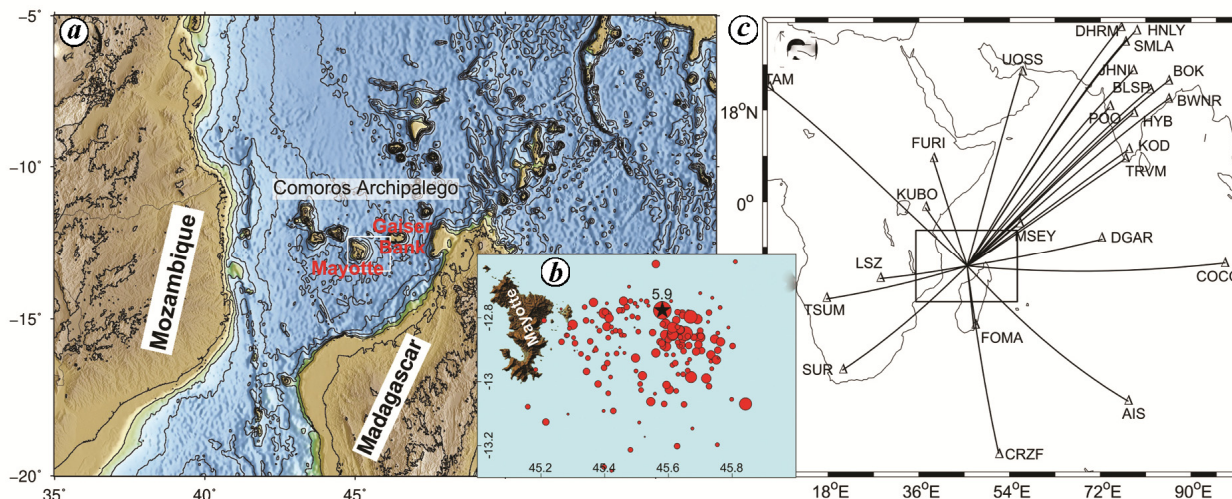


**Figure 1.** *a*, Map of Comoros archipelago and its neighbourhood with the bathymetry. *b*, Spatial distribution of the earthquake ( $m_b \geq 4$ ) swarm activity during May 2018–February 2019 from USGS. White rectangle around Mayotte in (*a*) shows the region considered in (*b*). The star shows the largest magnitude earthquake ( $M_w$  5.9) of the swarm that occurred on 15 May 2018. Initially this location was assumed as the source of the wave packets. *c*, Locations of seismic stations used with their standard codes whose latitude, longitude and names are available at the website of the International Seismological Centre.

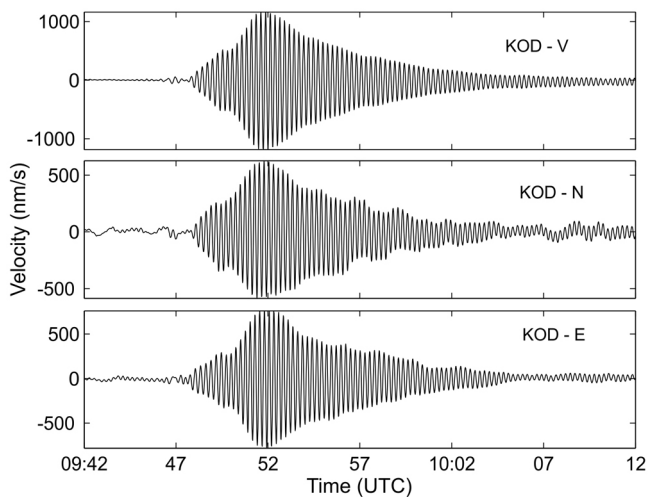


**Figure 2.** Vertical (V), north–south (N) and east–west (E) components of unfiltered ground velocity recorded at station KOD at 1 sample/sec. Note the difference in scales on the y-axis.

The absence of body waves prior to the surface wave-like wave packets of 11 November 2018 implies that either the source of the event has small magnitude or it is a slow, non-double couple event<sup>4</sup>. Yet, it is surprising that the wave packets were recorded worldwide; the waves were well-recorded at far-off stations, like Sierr La Laguna (SLBS), Baja California, Mexico at a distance of 154° from the source and at Pohakuloa (POHA), Hawaii, USA at a distance of 159°. Here we analyse the records of 11 November 2018 at seismic stations around Comoros archipelago (Figure 1 *c*) and also at other global stations to obtain some fundamental characteristics of the wave packets and their possible source.

## Data

We analysed broadband seismic data (flat velocity response at least up to 120 sec) pertaining to the 11 November 2018 event from seismic stations in the Indian region, acquired by the National Centre for Seismology, New Delhi along with data from Incorporated Research Institutions for Seismology (IRIS) at other global stations (Figure 1 *c*). We considered the data with 1 sample/sec, containing waves above period 2 sec. Figure 2 shows an example of three-component (V, N–S, E–W) unfiltered record at station KOD. To improve clarity in the signal, a bandpass filter 0.02–0.2 Hz was used. However, at some stations close to the Mayotte Island, noise was large in the frequency band 0.1–0.2 Hz, and so a band pass filter 0.02–0.1 Hz was required for clarity. In Figure 3 we display the filtered vertical-component seismograms at stations with varying azimuths and distances, where distance ( $\Delta$ ) is computed from the assumed source location as mentioned in the previous section.

## Wave characteristics

### Amplitude spectra

The period of waves in the seismograms did not change with time (Figures 2 and 3). We obtained amplitude spectra, which showed that the event at all 24 stations (Figure 3) had a dominant peak at period 15.63 sec, except at distant stations like POO, COCO and DHRM, where the peak was at 15.52, 15.75 and 15.75 sec respectively (Figures 4 and 5). Thus on average, the peak was at 15.6 sec. Other secondary peaks had spectral amplitudes less than one-tenth of the amplitude at 15.6 sec. Such sharp peaks,

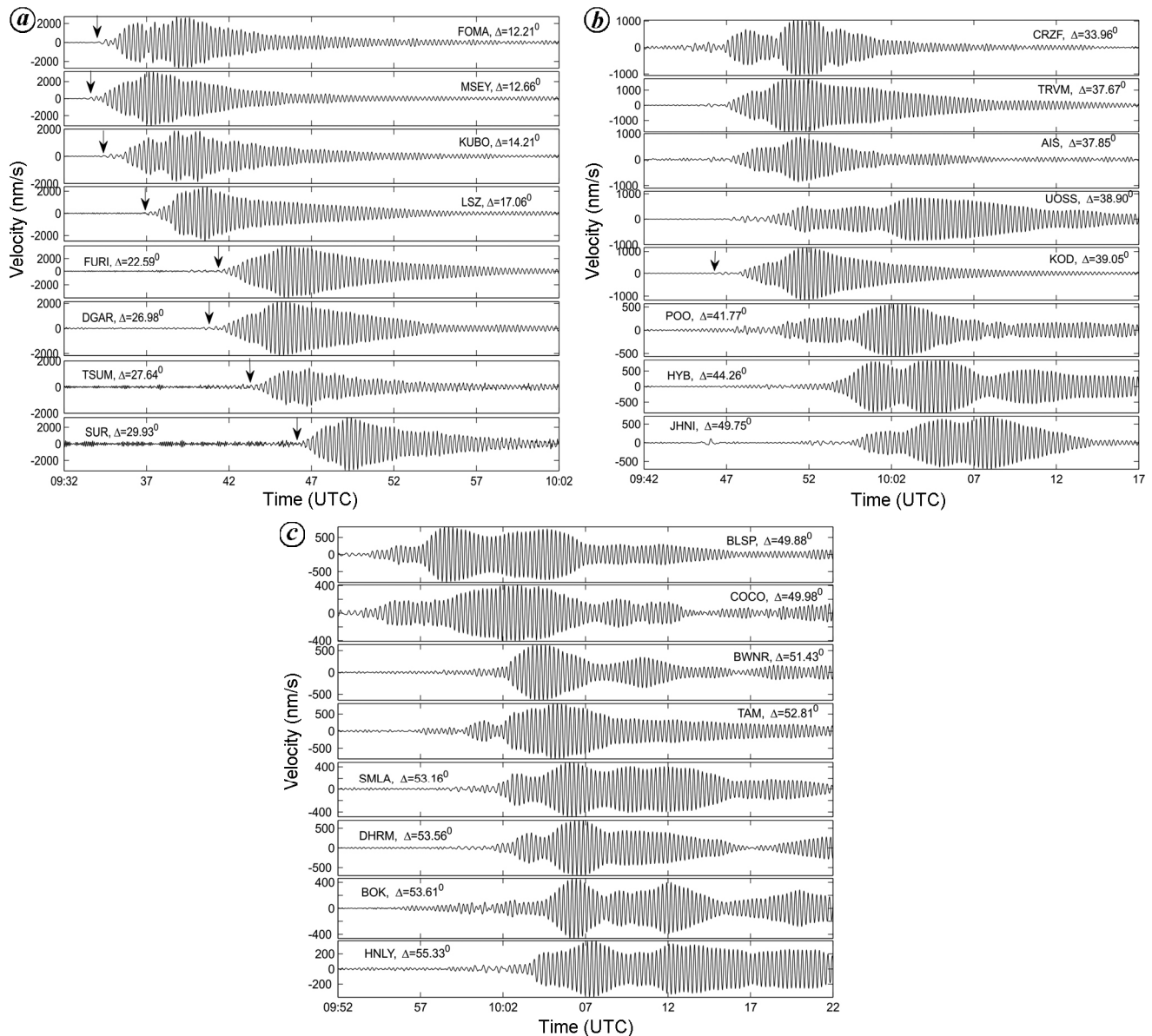


**Figure 3.** *a*, Vertical components of ground velocity waveform for stations  $\Delta < 30^\circ$  with common starting time as 09:32 UTC. Note the difference in scales on the y-axis. For clarity in waveform bandpass filter 0.02–0.2 Hz is used for stations LSZ, FURI, TSUZ, SUR and 0.02–0.1 Hz for FOMA, MSEY, KUBO and DGAR. Wherever possible, the beginning of the wave has been marked by an arrow. *b*, Same as (*a*), but for stations  $30^\circ < \Delta \leq 49.8^\circ$  with common starting time as 09:42 UTC. Bandpass filter 0.02–0.1 Hz is used for stations CRZF and AIS. For other stations filter 0.02–0.2 Hz is used. *c*, Same as (*a*) but for stations  $\Delta > 49.8^\circ$  with common starting time as 09:52 UTC. For all stations, bandpass filter 0.02–0.2 Hz is used.

present at all stations, suggest that the recorded waves of 11 November 2018 are monochromatic with period of 15.6 sec and thus are non-dispersive.

#### *Variation of amplitude with distance and azimuth*

The maximum in the amplitude envelopes of the wave packets, in general, decreased with distance in all directions from the assumed source (Figure 3). Further, amplitudes at nearly same distances were approximately same, irrespective of the direction, implying an isotropic nature

of the source. At short-distance stations ( $\Delta < 30^\circ$ , Figure 3 *a*) only one wave packet was recorded, whereas at many distant stations ( $\Delta > 30^\circ$ , Figure 3 *b* and *c*), two or three wave packets were recorded, which may be due to the arrival of waves from different wave paths<sup>5,6</sup>.

#### *Particle motion*

The three-component record showed that the wave packet arrived at the same time at all components and no other wave prior to this was seen in the horizontal component

(Figure 2). This indicates the presence of Rayleigh waves and absence of Love waves in the records. To confirm this further, we estimated the radial and transverse components at each station by rotating the N–S and E–W components for different back azimuths. We considered the back azimuth of a station as one which showed maximum amplitude in the radial component and minimum in the transverse component (Figure 6). The amplitudes in the transverse components at all stations were found to be significantly smaller than those in the vertical and radial components. This again confirms the absence of Love waves in the records. The estimated back azimuths were close to the direction of the assumed source.

Using the radial and vertical components, particle motion was drawn on a vertical plane through the wave path (Figure 7). The particle motion exhibited retrograde elliptic motion and further confirmed that wave packets are actually the Rayleigh waves. However, at a few stations the major axis of the ellipse was slightly tilted from the vertical, which may be due to some lateral heterogeneity around the stations<sup>7</sup>.

## Source characterization

### Origin time

For the near-source stations ( $\Delta < 30^\circ$ ), we could mark the arrival times of the wave packets quite unambiguously (Figure 3 *a*). However, at stations beyond  $30^\circ$  distance, unambiguous identification of arrival times of the wave packets was generally not possible, except at a station KOD (Figure 3 *b*). Azimuths from the source to stations MSEY and KOD were nearly the same (Figure 1 *b*). Between these two stations, the ratio of difference of

epicentral distances to the difference of arrival times was 3.9 km/s, which is close to the phase velocity of Rayleigh wave fundamental mode of period 15.6 sec along an oceanic path. The fundamental mode of Rayleigh wave was recorded since surface-wave amplitudes of this mode, in general, are large compared to other high modes. Considering that the wave packets have travelled at this speed, their arrival times at the nearby stations FOMA, MSEY and KOBO provide an average origin time of ~09:28 UTC on 11 November 2018.

### Source location

For estimating the location of the recorded wave packets, we used three nearby stations, namely FOMA ( $\Delta = 12.21^\circ$ ), MSEY ( $\Delta = 12.66^\circ$ ) and KOBO ( $\Delta = 14.21^\circ$ ), which form a triangle around the assumed source with nearly the same  $\Delta$  value (Figure 1 *b*). We observed that the arrival time at KUBO was 21 sec after FOMA, which is nearly in accordance with  $\Delta$  value of the two stations. However, arrival time at MSEY was 28 sec earlier than that at FOMA, although  $\Delta$  value was  $0.45^\circ$  more for the former. The difference in arrival times may be due to the difference in the Rayleigh wave speed along the two wave paths. However, to accommodate a part of the arrival time difference, the actual source location may be about  $0.2^\circ$  towards northeast of the assumed location. With such a shift, the source was estimated to be located at the northeastern edge of the swarm zone (Figure 1 *b*), which corresponds to a location between the Mayotte island and Geiser bank.

### Mechanism

In the recorded seismograms of the event, the *P*- and *S*-waves were not visible but Rayleigh waves were clear and non-dispersive. To explore this theoretically, synthetic seismograms were generated using the PREM earth model<sup>8</sup>. In this model, the ocean thickness is assumed as 3 km. Synthetic seismograms were obtained at the bottom of ocean following Bhattacharya<sup>9</sup>. We assumed an isotropic source at 15 km depth with a monochromatic time-derivative source–time–function of period 16 sec (Figure 8 *a*). The assumption of isotropic source was based on observations that the seismograms had no Love waves but only Rayleigh waves, whose amplitude was nearly the same at the same distances in all azimuths.

Figures 8 *b* and *c* shows the vertical and radial components of synthetic seismograms at epicentral distances  $20^\circ$  and  $50^\circ$ . We do not show the transverse components whose amplitudes are zero in these synthetics, consistent with the relatively smaller amplitude observed in the transverse component (Figure 6) at all stations. Synthetic seismograms show that not only are *P*- and *S*-waves weak, but also the Rayleigh wave amplitudes are relatively

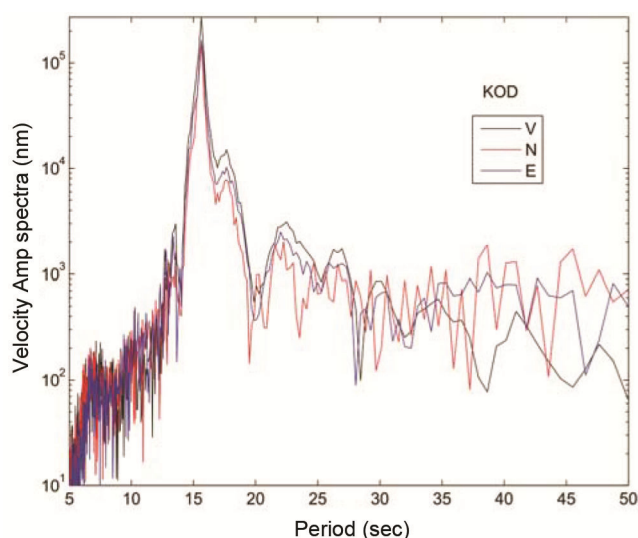


**Figure 4.** Amplitude spectra of ground velocity of V, N and E components at station KOD.

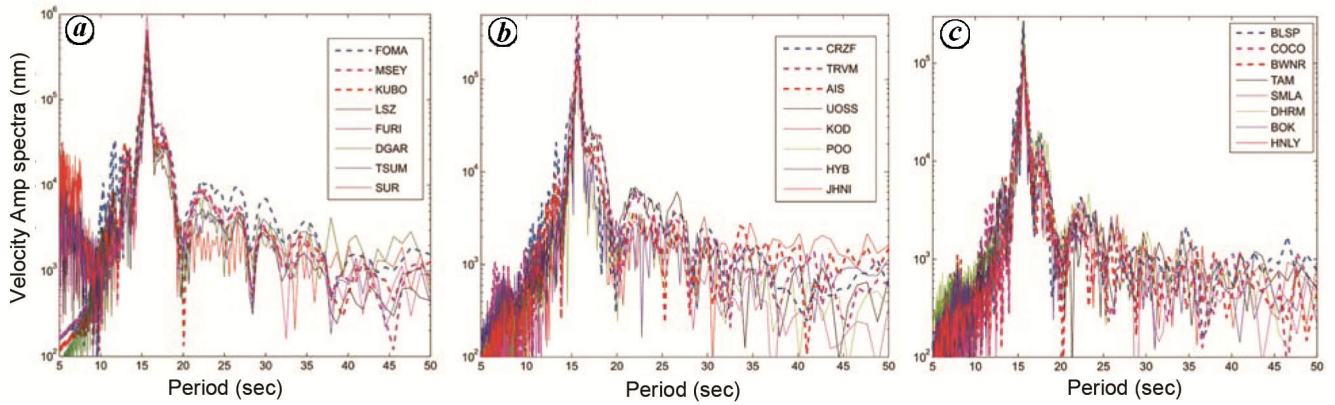


**Figure 5.** *a*, Amplitude spectra of velocity of the vertical components of stations in Figure 3 *a*. *b*, Same as (*a*), but for stations in Figure 3 *b*. *c*, Same as (*a*), but for stations in Figure 3 *c*.

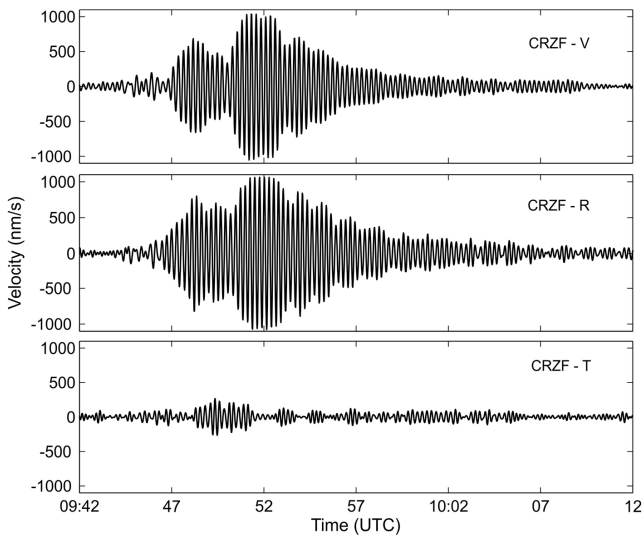


**Figure 6.** Vertical (V), radial (R) and transverse (T) components at station CRZF. Scale is the same for all the three-components. The amplitude in the T-component is significantly small compared to the V- and R-components.

large. However, with increase in focal depth, the amplitudes of *P*- and *S*-waves increase relative to those of Rayleigh waves. Thus instead of keeping the focal depth too shallow, an optimum focal depth is obtained so that body wave amplitudes remain relatively smaller. The amplitude spectra of synthetics show sharp peak at 16.0 sec. Thus the waves in synthetic seismograms at stations are monochromatic of similar period as that of the source–time–function. The synthetics in Figure 8 *b* and *c* show similarity with the observed seismograms (Figure 3).

As seen in the waveforms at stations LSZ ( $\Delta = 17.06^\circ$ ) and FURI ( $\Delta = 22.59^\circ$ ) in Figure 3 *a*, the average observed maximum amplitude at  $\Delta \sim 20^\circ$  is about 3000 nm/s. Further, using the waveforms of JHNI ( $\Delta = 49.75^\circ$ ), BLSP ( $\Delta = 49.88^\circ$ ), COCO ( $\Delta = 49.98^\circ$ ) and BWNR ( $\Delta = 51.40^\circ$ ) in Figure 3 *b* and *c*, the average observed maximum

amplitude at  $\Delta \sim 50^\circ$  is about 800 nm/s. To achieve nearly the same amplitude in synthetics at these distances, we have considered seismic moment ( $M_0$ ) as  $1.50 \times 10^{23}$  dyn cm for the source and this corresponds to  $M_W = 4.8$ . However, this is an approximate estimate as we are not using an exact earth structure along the wave path.

The time-derivative of source–time–function in Figure 8 *a* implies that we have considered a transient oscillation at the isotropic source. This is similar to the radial oscillation of a fluid-filled sphere considered by Fujita *et al.*<sup>10</sup> for the source mechanism of a harmonic volcanic tremor. They considered a fluid-filled sphere of radius  $r_0$  with density  $\rho_1$  and *P*-wave velocity  $\alpha_1$ , embedded in an infinite Poisson solid medium with density  $\rho_2$  and *P*-wave velocity  $\alpha_2$ . Using the equation of motion and boundary conditions they derived an equation to evaluate eigen frequencies in terms of  $\Omega = \omega(r_0/\alpha_1)$ , where  $\omega$  is the angular frequency. Thus the radius of the sphere is

$$r_0 = \alpha_1 \Omega / \omega, \quad (1)$$

Model 2 of Fujita *et al.*<sup>10</sup> gives the average parameters of the sphere of the volcanic fluid. In this model,  $\alpha_2/\alpha_1 = 5.49$ ,  $\rho_2/\rho_1 = 2.0$  and  $\alpha_1 = 0.4552$  km/s, which gives the eigen frequency as  $\text{Re}(\Omega) \cong 4.3$  for the fundamental mode (which has higher amplitude than other higher modes) of oscillation. In the present case,  $\omega = 2\pi/15.6 \text{ s}^{-1}$  and considering the model 2 for our source region, eq. (1) gives  $r_0 = 4.9$  km, which suggests that radial oscillations of the fluid-filled sphere of  $\sim 5$  km radius generated the wave packets.

## Discussion

Low-frequency or long-period (LP) seismic events are recorded from volcanic regions in many parts of the world<sup>11</sup> and their frequency normally varies between 0.5 and 5 Hz (ref. 12), with their duration less than 1 min.

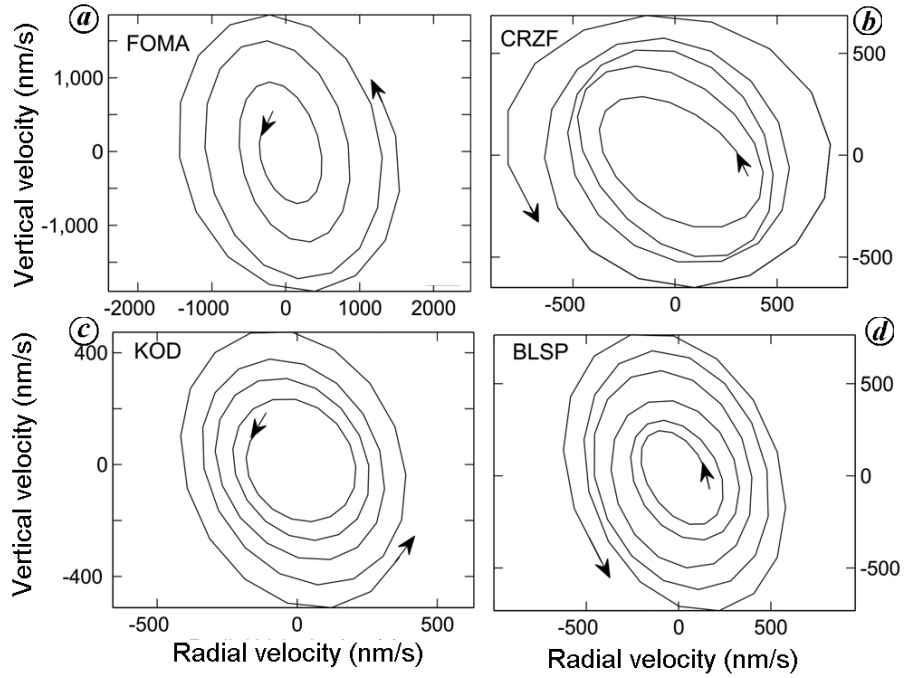


**Figure 7.** Particle motion on the vertical plane through the wave path: for stations (a) FOMA (plotted from 09:35:08 to 09:36:10 UTC), (b) CRZF (plotted from 09:47:01 to 09:48:16 UTC) (c) KOD (plotted from 09:48:11 to 09:49:27 UTC) and (d) BLSP (plotted from 09:56:50 to 09:58:18 UTC) showing retrograde elliptic motion. For clarity, particle motion is drawn for limited part of the wave when the amplitudes are increasing.

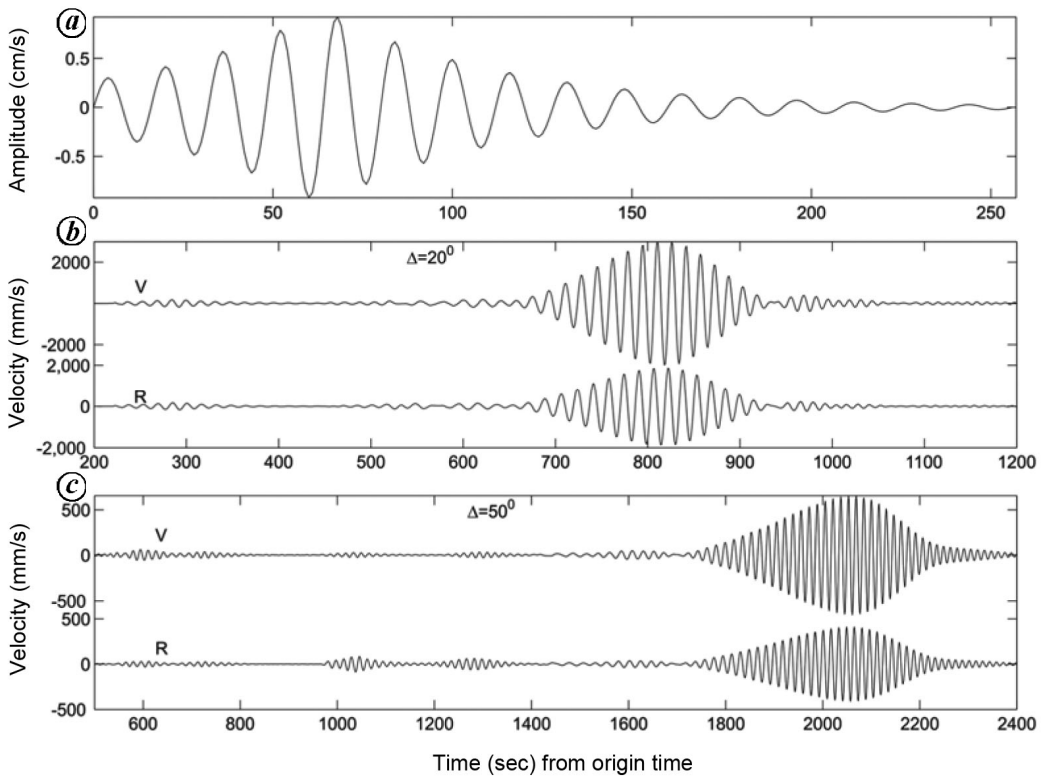


**Figure 8.** a, Time derivative of source–time–function, which is an amplitude-varying sine wave of period 16 sec and duration 256 sec. Source is at 15 km depth with  $M_0 = 1.5 \times 10^{23}$  dyn cm. b and c, Vertical (V) and radial (R) synthetic seismograms using PREM at epicentral distance of (b)  $20^\circ$  and (c)  $50^\circ$ . Rayleigh waves (wave packets) in synthetics are of the same period as that of the source–time–function and are of much larger amplitude compared to the P- and S-waves. The transverse components have zero amplitude for the source considered here and hence are not shown.

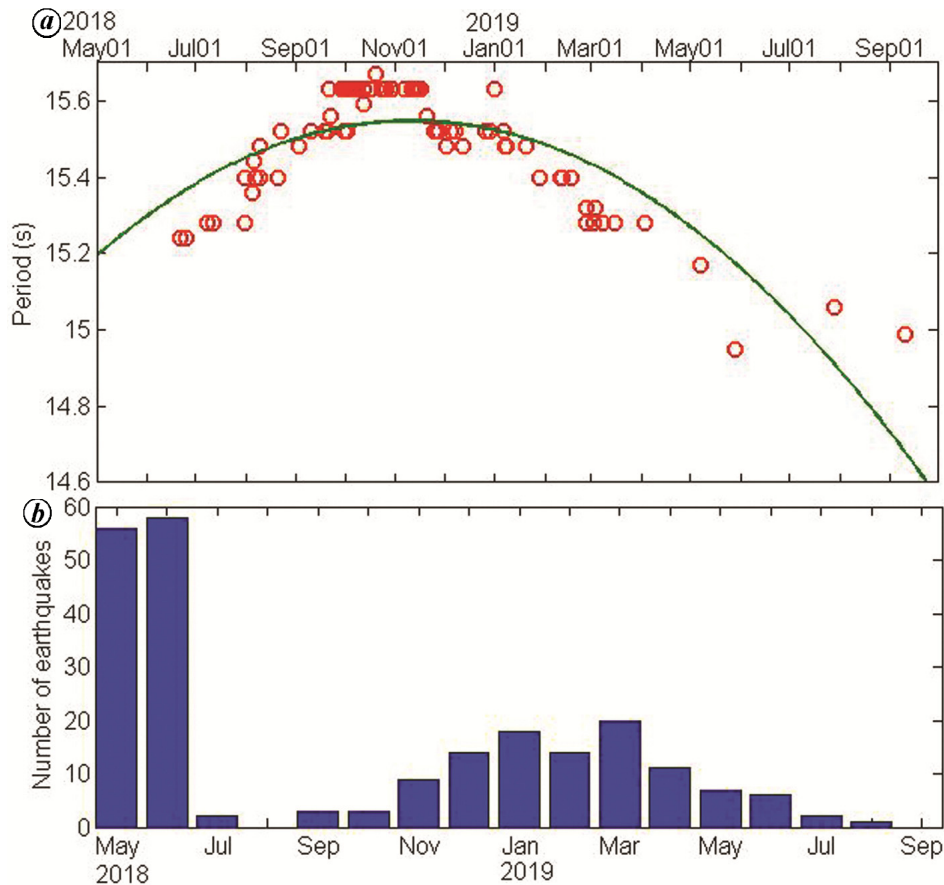


**Figure 9.** *a*, Small red circles show periods of monochromatic waves on different dates. Green curve shows a least square quadratic fit to the data. *b*, Number of earthquakes reported by USGS of magnitude 4 and above per month in the swarm area (Figure 1 *b*).

Further, such waves have rarely been recorded beyond 100 km. The difference between the earlier observations and the present one is in the frequency content, the duration of waveform and the distance at which they are observed. However, Talandier *et al.*<sup>13</sup> analysed two seismic events of May 2011 and April 2013 generating monochromatic Rayleigh waves of period 17 sec and duration of about 40 min, which were recorded only at regional distances. These events probably originated from a hot spot of Rocard submarine volcano in southern Pacific, about 100 km east of Tahiti. The present case is anomalous in the sense that waveforms are recorded worldwide and such monochromatic Rayleigh waves have been recorded on many occasions at large distances since June 2018 from the same source with slight increase and decrease in periods (Figure 9 *a*).

These LP harmonic waveforms are interpreted as oscillations of a fluid-filled resonator. As a possible origin of the 17 sec period Rayleigh waves, Talandier *et al.*<sup>13</sup> proposed that the entire volcanic conduit might have vibrated during the ejection of lava and resonated to generate the monochromatic Rayleigh waves. Although many geometries are possible for a source resonator<sup>11,12</sup>, we considered a

fluid-filled sphere as the resonator because a sphere is one of the simplest shapes in nature and radial oscillations of a sphere act as an isotropic source which, in this case, is required to fit the observations. Gudmundsson<sup>14</sup> noted that some magma chambers become spherical due to isotropic and close-to-isotropic stress. Such geometry may also occur directly from cooling of a differently shaped chamber<sup>14,15</sup>. With a radial oscillation of such a spherical source, we have generated synthetic seismograms which consist of wave packets with non-dispersive Rayleigh waves and relatively negligible body wave amplitude, consistent with the observations. The size of the fluid sphere is estimated to be large compared to the previous findings<sup>10</sup>; but a large size is needed to have ultra-LP oscillations of period 15.6 sec. We assumed a point source while generating synthetic seismograms, because the diameter of the fluid sphere is negligible compared to the epicentral distances considered here.

It is interesting to note here that since 21 June 2018, similar monochromatic waves from the same source have been recorded at nearby stations such as FOMA, MSEY, KMBO and LSZ; however, amplitudes of these waves are smaller than those of 11 November 2018. Such

occurrences are more during October and early November 2018 (Figure 9a). As before, the period of the monochromatic waves is derived from the sharp peak of amplitude spectra and it increased from 15.24 sec on 21 June 2018 to 15.63 during October and early November 2018. However, the period started decreasing from 20 November 2018 and reached 15.0 sec on 10 September 2019 (Figure 9a). Using eq. (1) and considering no change of material within the fluid sphere, this increase and decrease in period indicate that the radius of the fluid sphere increased from 4.7 to 4.9 km and again decreased to 4.7 km. It appears that the decrease in period or shrinking of the fluid sphere occurs along with decrease of swarm activity (Figure 9b).

## Conclusion

(1) The particle motion and the wave speed show that the observed wave packets are fundamental mode Rayleigh waves. Further, the amplitude spectra showed that the waves are monochromatic and non-dispersive. Transverse components of the wave packet show the absence of Love waves.

(2) At nearby stations, single wave packet was recorded, whereas at some distant stations multiple packets were recorded which were possibly caused by multi-pathing.

(3) The source of the event is located at the northeastern edge of Mayotte earthquake swarm zone, which started in May 2018.

(4) The recorded monochromatic wave packets with a period of 15.6 sec are consistent with the synthetic seismograms for an isotropic source at  $\sim 15$  km depth with a transient oscillation of the same period. Comparison of amplitudes between the observed and synthetic seismograms implies an  $M_w$  of  $\sim 4.8$  for the source.

(5) Considering source of the event as a volcanic fluid-filled sphere oscillating radially with a period of 15.6 sec, the radius of the sphere is estimated to be  $\sim 5$  km.

(5) Similar monochromatic Rayleigh waves with lesser amplitudes have been recorded on several occasions from 21 June 2018 to 10 September 2019. The period of the waves increased till October and early November 2018 and then decreased from 20 November 2018, which implies an increase and then decrease in the radius of the fluid sphere.

1. Esson, J., Flower, F. J., Strong, D. F., Upton, B. G. J. and Wadsworth, W. J., Geology of the Comoros archipelago, western Indian Ocean. *Geol. Mag.*, 1970, **107**, 549–557.
2. Michon, L., The volcanism of the Comoros archipelago integrated at a regional scale. In *Active Volcanoes of the Southwest Indian Ocean* (eds Bachelery P. et al.), Springer, 2016, pp. 333–344; doi:10.1007/978-3-642-31395-0\_21.
3. Bachèlery, P., Morin, J., Villeneuve, N., Soulé, H., Nassor, H. and Ali, A. R., Structure and eruptive history of Karthala volcano. In *Active Volcanoes of the Southwest Indian Ocean* (eds Bachèlery, P. et al.), Springer, Berlin, Heidelberg, 2016, pp. 345–366; doi:10.1007/978-3-642-31395-0\_22.
4. Ito, Y., Obara, K., Shiomi, K., Sekine, S. and Hirose, H., Slow earthquakes coincident with episodic tremors and slow slip events. *Science*, 2007, **315**, 503–506.
5. Capon, J., Analysis of Rayleigh-wave multipath propagation at LASA. *Bull. Seismol. Soc. Am.*, 1970, **60**, 1701–1731.
6. Ji, C., Tsuboi, S., Komatitsch, D. and Tromp, J., Rayleigh-wave multipathing along west coast of North America. *Bull. Seismol. Soc. Am.*, 2005, **95**, 2115–2124.
7. Wang, J. H. and Wu, F. T., Numerical particle motion of Rayleigh waves in laterally inhomogeneous media. *J. Phys. Earth*, 1989, **37**, 325–343.
8. Dziewonski, A. M. and Anderson, D. L., Preliminary reference Earth model. *Phys. Earth Planet. Inter.*, 1981, **25**, 297–356.
9. Bhattacharya, S. N., Synthetic seismograms in a spherical Earth using exact flattening transformation. *Geophys. Res. Lett.*, 2005, **32**, L21303, doi:10.1029/2005GL02452.
10. Fujita, E., Ida, Y. and Oikawa, J., Eigen oscillation of a fluid sphere and source mechanism of harmonic volcanic tremor. *J. Volcanol. Geotherm. Res.*, 1995, **69**, 365–378.
11. Cauchie, L., Saccorotti, G. and Bean, C. J., Amplitude and recurrence time analysis of LP activity at Mount Etna, Italy. *J. Geophys. Res.*, 2015, **120**, 6474–6486; doi:10.1002/2015JB011897.
12. Crosson, R. S. and Bame, D. A., A spherical source model for low frequency volcanic earthquakes. *J. Geophys. Res.*, 1985, **90**, 10237–10247.
13. Talandier, J., Hyvernaud, O. and Maury, R. C., Unusual seismic activity in 2011 and 2013 at the submarine volcano Rocard, Society hot spot (French Polynesia). *Geophys. Res. Lett.*, 2016, **43**, 4247–4254; doi:10.1002/2016GL068342.
14. Gudmundsson, A., Magma chambers: formation, local stresses, excess pressures and compartment. *J. Volcanol. Geotherm. Res.*, 2012, **237–238**, 19–41.
15. Gudmundsson, A., Emplacement of dykes, sills and crustal magma chambers at divergent plate boundaries. *Tectonophysics*, 1990, **176**, 257–275.

ACKNOWLEDGEMENTS. We thank the two anonymous reviewers for their constructive comments. This is NGRI publication number NGRI/Lib/2019/Pub-80.

Received 30 April 2019; revised accepted 19 October 2019

doi: 10.18520/cs/v118/i7/1069-1076